Magnetic ordering effects in the mixed induced-moment ferromagnetic diamagnetic system $RbFe_{(1-x)}Mg_xCl_3$

1990 J. Phys.: Condens. Matter 2 10487

(http://iopscience.iop.org/0953-8984/2/51/020)

J. Phys.: Condens. Matter 2 (1990) 10487–10500. Printed in the UK

Magnetic ordering effects in the mixed induced-moment ferromagnetic diamagnetic system $RbFe_{(1-x)}Mg_xCl_3$

A Harrison and D Visser†

Oxford University, Inorganic Chemistry Laboratory, South Parks Road, Oxford, OX1 3QR, UK

Received 25 June 1990

Abstract. Elastic neutron scattering experiments were performed on single crystals of the solid solution $RbFe_{(1-x)}Mg_xCl_3$ ($x = 0.02$, 0.03 and 0.05) to study the influence of diamagnetic dilution on the magnetic ordering processes of the induced-moment, pseudo-one-dimensional ferromagnet $RbFeCl_3$. All the samples appeared to have finite-range magnetic correlations with ordering vectors similar to those of the commensurate, C, and the two incommensurate magnetic phases, IC_1 and IC_2, of pure $RbFeCl_3$. The $x = 0.02$ and 0.03 samples showed transitions from the paramagnetic to the IC_1 phase at the same temperature of 2.55 K, then transitions to the IC_2 and C phases at temperatures that decreased sharply with x. The $x = 0.05$ sample also showed a transition to the IC_1 phase at 2.55 K, but no further transitions down to the lowest experimental temperature of 1.38 K. All samples showed an additional elastic diffuse magnetic scattering component centred at the commensurate magnetic ordering vector $(\frac{1}{3}\ \frac{1}{3}\ 0)_N$. This diffuse component became broader and weaker as x increased from 0.02 to 0.05 and as the sample was warmed, but persisted until about 10 K.

1. Introduction

This paper follows recent work on the inhomogeneous magnetic materials $Rb_{(1-x)}Cs_xFeCl_3$ (Harrison *et al* 1986), which is a mixed magnetic–singlet ground state material, and $RbFeCl_{(3-x)}Br_x$ (Harrison and Visser 1989), which is a mixed induced-moment ferromagnetic–antiferromagnetic material. We will henceforth refer to these two works as I and II respectively. In order to demonstrate the motivation for the present work it is necessary to consider briefly the delicate balance of competing influences that govern the magnetic behaviour of the pure compounds $AFeX_3$ (A = Rb, Cs; X = Cl, Br). Fuller reviews are given in Lines and Eibschutz (1975), Eibschutz *et al* (1975) and II.

All of these materials have a hexagonal perovskite structure (space group $P6_3/mmc$) in which chains of face-sharing FeX_6^{4-} octahedra lie parallel to the crystal c axis. The chain structure leads to pseudo-one-dimensional magnetic behaviour: the intrachain magnetic exchange constant J_1 is an order of magnitude greater than the interchain magnetic exchange constant J_2. J_2 is antiferromagnetic for all the $AFeX_3$ compounds, but the sign of J_1 depends on the Fe–X–Fe intrachain superexchange bridge angle α: the bromides are found to have antiferromagnetic J_1, whereas the chlorides, with larger α, have ferromagnetic J_1.

The single-ion electronic ground state of isolated Fe^{2+} ions in the trigonally-distorted

† Present address: Department of Physics, Loughborough University of Technology, Loughborough, LE11 3TU, UK.

0953-8984/90/5110487+14$03.50

octahedral ligand field environment in these materials would be a singlet, $|m_J = 0\rangle$, with a low-lying excited doublet, $|m_J = \pm 1\rangle$, at an energy D. Perturbation of this three-level system through magnetic superexchange or a magnetic field applied parallel to the crystal c axis can induce a magnetic ground state. In zero applied magnetic field the rubidium salts show magnetic long-range ordering at low temperatures, whereas the caesium salts, with larger unit cells, and smaller magnetic exchange interactions, show true singlet ground state character.

A third form of competition between different types of magnetic behaviour exists in the chlorides, in which the ferromagnetic intrachain correlations lead to an appreciable interchain magnetic dipole–dipole interaction, γ (Shiba 1982, Shiba and Suzuki 1983). The exchange field provided by J_2 favours a free-energy minimum at the K point of the hexagonal reciprocal lattice ($\boldsymbol{Q} = (\frac{1}{3}\ \frac{1}{3}\ 0)_N$), whereas γ favours a minimum at the M point ($\boldsymbol{Q} = (\frac{1}{2}\ 0\ 0)_N$ and equivalent positions). Competition between J_2 and γ in pure $RbFeCl_3$ leads to the formation of two incommensurate magnetic phases, IC_1 and IC_2, as it is cooled from the paramagnetic phase to 2.55 and 2.35 K respectively. The commensurate magnetic phase, C, which has 120° antiferromagnetic order in the triangular basal plane, forms at 1.95 K (Wada *et al* 1982).

The mixed singlet-magnetic ground state compounds $Rb_{(1-x)}Cs_xFeCl_3$ were studied by single-crystal neutron diffraction and their magnetic structures found to be very dependent on the composition x, temperature and magnetic field applied parallel to the c axis (I). In particular, the magnetic ordering observed in the pure rubidium salt was found to be destroyed on the addition of small concentrations of $CsFeCl_3$, and the degree of magnetic inhomogeneity found to decrease strongly as a magnetic field was applied parallel to the c axis. Distinct differences were found between the zero-field-cooled, and the field-cooled sublattice magnetization.

The mixed ferromagnet–antiferromagnet $RbFeCl_{(3-x)}Br_x$ was also studied by single-crystal neutron diffraction (II) in order to investigate the possibility of forming a spin-glass phase at intermediate composition (Fishman and Aharony 1979, Bontemps *et al* 1982, Katsumata *et al* 1982, and Munninghof *et al* 1984). However, the induced-moment character of these materials sensitizes them towards impurities: 1 or 2% of the dopant $RbFeBr_3$ was sufficient to destroy the magnetic long-range order in $RbFeCl_3$. At intermediate composition the magnetic phase was best described as a singlet ground state material with random intrachain magnetic exchange.

In both mixed systems the neutron scattering maxima near the magnetic Bragg positions of the pure compounds were greater than the instrumental resolution width, corresponding to magnetic correlations of *finite* range. It was not possible to explain this satisfactorily using existing models. In addition to the relatively sharp scattering maxima in the mixed compounds, a diffuse scattering component was observed at the same positions, but persisting to higher temperatures. The origin of this effect was also uncertain.

It is difficult to treat either of these systems at a microscopic level because of the complexity of the structural or magnetic disturbances produced by the impurities. It is *likely* that Cs^+ produces a shell of structural distortions, accompanied by a reduction in the magnitude of the induced moments on some of the neighbouring iron atoms. Doping $RbFeCl_3$ with Br^- gives rise to superexchange bridges of various compositions, with indeterminate exchange constants J_{ij}. By doping $RbMgCl_3$ into $RbFeCl_3$ we exchange Fe^{2+} ions for the diamagnetic Mg^{2+}, and produce an inhomogeneous magnet in which the microscopic picture might be clearer. In addition, the substitution of Fe^{2+} by Mg^{2+} is expected to have a less disruptive influence on the the crystal structure, and consequently on the superexchange pathways, than the substitution of Rb^+ by Cs^+ or Cl^- by Br^-. In the present paper we report a single-crystal neutron diffraction study of the magnetic ordering of $RbFe_{(1-x)}Mg_xCl_3$ for small values of x ($0 < x < 0.05$) with the aim of clarifying some of the disordering effects in the Rb–Cs and Cl–Br mixed compounds.

2. Experimental method

All the samples used in these experiments were prepared in precisely the same manner as the $RbFeCl_{(3-x)}Br_x$ compounds, as described in II. $MgCl_2$ was prepared from the Analar grade hydrate, $MgCl_2.6H_2O$. Analysis of the magnesium and iron contents of the boules by flame photometry revealed them to be homogeneous down their entire lengths to within 5% of the nominal concentration of Mg^{2+}.

Small parts of the boules of the mixed compounds were checked with x-ray powder diffraction to establish their homogeneity and crystal structure. $RbMgCl_3$ crystallizes in a slightly different structure (Seifert and Fink 1975) to $RbFeCl_3$ with a hexagonal–cubic (HC) anion stacking sequence, space group $P6_3/mmc$ and unit cell dimensions $a = 7.090$ Å and $c = 11.844$ Å. It was thought possible that the Mg^{2+} impurities could induce stacking faults. The diffraction patterns of the mixed compounds could be fully indexed on the simple hexagonal unit cell of $RbFeCl_3$, for which the space group is $P6_3/mmc$ and the unit cell dimensions are $a = 7.100$ Å and $c = 6.048$ Å (II). A careful investigation of the background scattering in the powder diffraction patterns showed no indications of a HC-type crystal structure, nor were there any indications of line-broadening effects due to HC stacking faults as observed in $TlFeCl_3$ (Zodkevitz *et al* 1970). We may conclude that small concentrations of $RbMgCl_3$ form a solid solution with $RbFeCl_3$.

Samples, typically measuring $3 \times 3 \times 5$ mm^3, were cleft from the boules and mounted with the $(100)_N$ and $(220)_N$ reflections in the horizontal scattering plane. Neutron diffraction was performed on samples of $RbFe_{(1-x)}Mg_xCl_3$ of composition $x = 0.02$ and $x = 0.05$ on the two-axis diffractometer D15 at the ILL (Institut Laue–Langevin), at a neutron wavelength of 1.174 Å. Temperatures down to 1.3 K were provided by an ILL 'Orange' cryostat. Collimation before and after the sample was provided by two sets of apertures measuring 12 mm square. The divergence of the neutron beam was 1° at the sample. The instrumental resolution function at the K point of the mixed samples was determined by measuring the width of the same magnetic Bragg peak in a sample of pure $RbFeCl_3$. The widths of the nuclear Bragg peaks in the sample of pure $RbFeCl_3$ lay within 10% of those of the same nuclear Bragg peaks in the $RbFe_{(1-x)}Mg_xCl_3$ samples used in the present measurements when those peaks were scanned in both a tangential (ω scan) and a radial fashion ($(\omega - 2\theta)$ scan).

The scattered neutron intensity was then mapped in the regions of the K point and the M point of the hexagonal reciprocal lattice as a function of temperature. These measurements revealed satellite peaks centred on the K point at low temperatures, plus an additional diffuse scattering component centred at that point, which persisted to higher temperatures. These results prompted a second study using an instrument of higher spatial resolution, with energy resolution and a lower background count. The neutron scattering study of the sample of composition $x = 0.03$ was carried out on the triple-axis diffractometer D10 at the ILL at a wavelength of 2.363 Å. The spectrometer was set up to detect elastically scattered neutrons. The full width at half maximum of the Bragg peak at $Q = (\frac{1}{3}\ \frac{1}{3}\ 0)$ equalled 0.7° in ω.

3. Results

The scattered neutron intensity from all samples revealed maxima at or around the K point, corresponding to magnetic correlations similar to those found in pure $RbFeCl_3$ (figure 1). Scans were made through the K point along the KM direction and also perpendicular to the $[110]_N$ direction. These maxima were fitted to a variety of lineshape functions, as described in II. In all cases the best least-squares fit was found for Lorentzian curves convoluted with the

Gaussian resolution function. As with the $RbFeCl_{(3-x)}Br_x$ compounds the analysis was complicated by the appearance of a broad, weak maximum centred at the K point which persisted to 6–10 K. There was the additional complication of uncertainty in the instrumental resolution width near the K point.

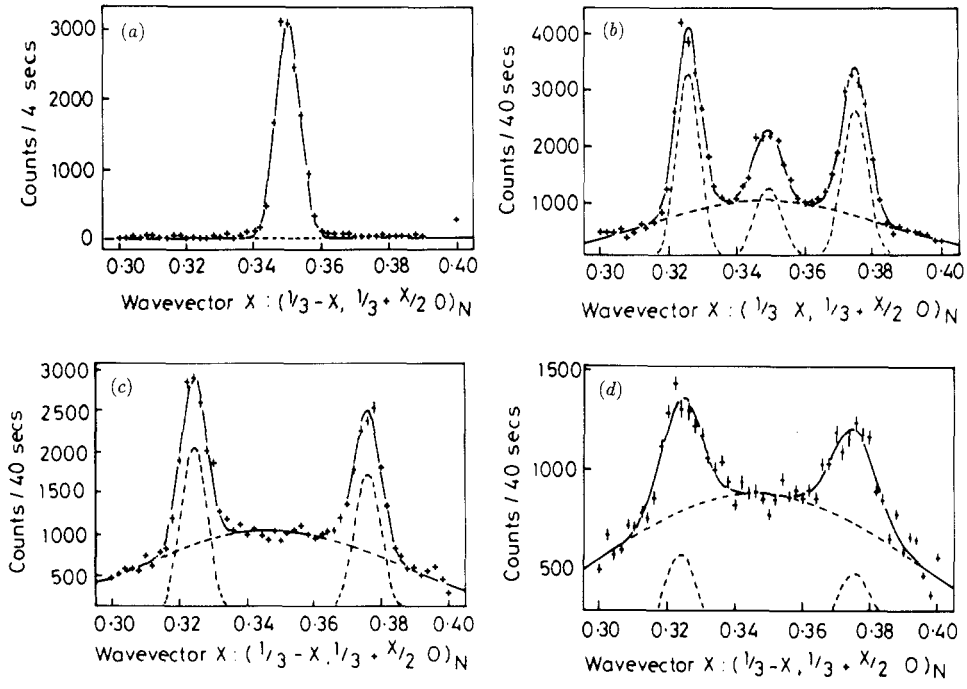

Figure 1. Examples of the diffuse scattering component in the $x = 0.02$ sample at (*a*) 1.32 K, (*b*) 2.15 K, (*c*) 2.24 K and (*d*) 2.34 K. The full curves in figures 1(*b*)–(*d*) represent the best fits to the background-corrected data of Lorentzian curves convoluted with the Gaussian resolution function, and the broken curves give the separate contributions, clearly showing the diffuse part. In figure 1(*a*) the full curve does *not* include the diffuse component, demonstrating how the it was first detected.

Magnetization curves for all the doped samples, measured at $\boldsymbol{Q} = (\frac{1}{3}\ \frac{1}{3}\ 0)_N$, are presented in figures 2(*a*) and (*b*). The magnetization curve for pure $RbFeCl_3$, taken on instrument D15 at the same wavelength as the measurements made on the $x = 0.02$ and $x = 0.05$ samples, is presented for comparison. Data for the $x = 0.02$ and 0.05 samples have been scaled against the intensities of the respective $(110)_N$ reflections. The scaling of intensities for different samples should also take into account the different structure factors of the nuclear peaks used for normalization. However, over the composition range considered here this change is expected to be very small (I, II).

These curves clearly demonstrate the successive paramagnetic–IC–C phase transitions in the pure and $x = 0.02$ and 0.03 samples, and this is confirmed by the form of the satellite and central Bragg peaks in and around the K point. However, the $x = 0.05$ sample only exhibited the satellite structure indicative of magnetic correlations with an IC_1-type periodicity below 2.55 K and down to the lowest experimental temperature of 1.38 K.

The displacement of the satellite peaks in the IC_2- and IC_1-like phases increased with temperature and concentration of dopant as illustrated in figure 3. This result is very similar to those for $Rb_{(1-x)}Cs_xFeCl_3$ and $RbFeCl_{(3-x)}Br_x$, with the satellite displacement at higher

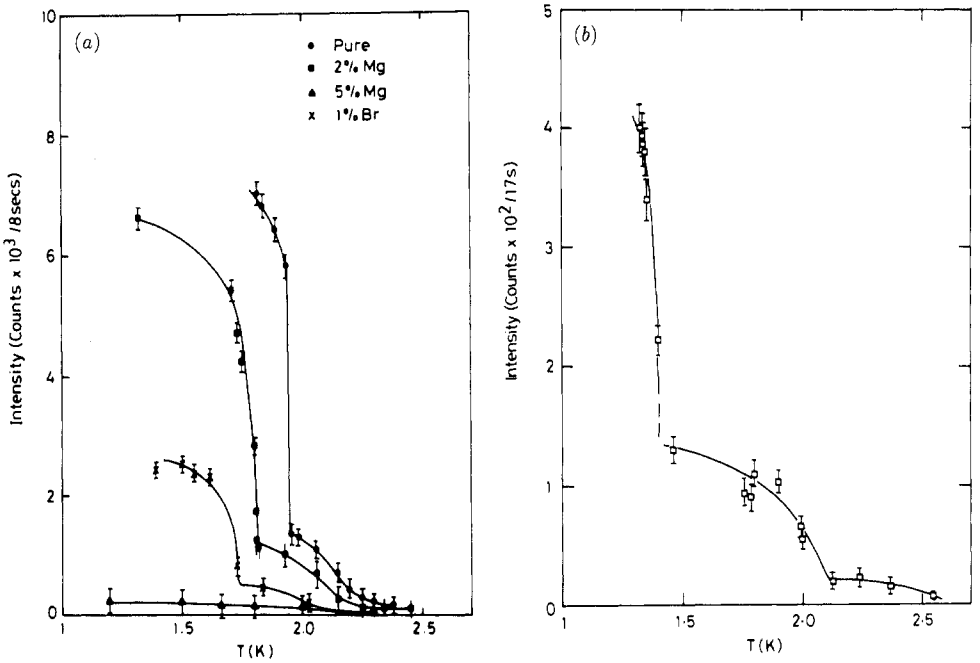

Figure 2. The temperature dependence of the magnetization measured at the K point for samples of $RbFe_{(1-x)}Mg_xCl_3$ of (*a*) composition $x = 0.02$ and 0.05 and (*b*) composition $x = 0.03$. The data for the $x = 0.02$ and 0.05 samples have been scaled against each other using the intensities of the nuclear (110) and (220) reflections. The result of a similar measurement (I) on $RbFeCl_{(3-x)}Br_x$ ($x = 0.03$) is included for comparison. The data for the $x = 0.03$ sample were scaled in a similar manner, and a further correction was also made for the change in neutron wavelength.

temperatures (≈ 2.5 K) tending to a similar asymptotic value ($\delta R \approx 2.5 \times 10^{-2}\ 2\pi/a$ Å^{-1}).

The widths of the neutron scattering maxima for all the samples increased as the concentration of dopant was increased (figure 4). The pure and $x = 0.02$ samples had peak widths which were independent of temperature through all the ordered magnetic phases: the peak widths of the $x = 0.02$ sample lay within the experimental uncertainty in the resolution width so it is quite possible that they are also resolution limited, as has been established for pure $RbFeCl_3$ (II). The $x = 0.05$ sample, and to a lesser degree the $x = 0.03$ sample, showed a monotonic increase in peak width with temperature.

The diffuse scattering component centred at the K point, seen in addition to the relatively sharp scattering maxima described above, clearly persisted above 2.5 K in the $x = 0.02$ and $x = 0.05$ samples; it was less distinct above 2.55 K in the measurements made on the $x = 0.03$ sample on the triple-axis spectrometer D10. This was probably due to the different experimental set-up for this sample. However, the measurements made with D10 *did* show that the diffuse component is primarily elastic in origin and has little, if any, contribution from low-energy magnetic fluctuations. Furthermore, the intensity of the scattering continued to rise as the temperature was lowered from T_N, which is contrary to what would be expected for quasi-elastic scattering.

More detailed information about the additional diffuse component below T_N could only be obtained for the $x = 0.02$ sample in which the diffuse component is most intense. The data were fitted to Lorentzian curves convoluted with the Gaussian resolution function describing

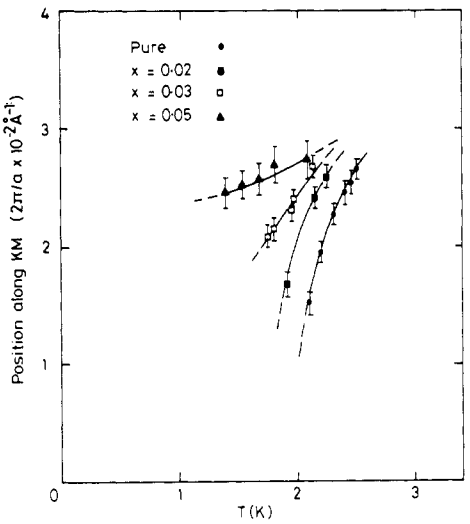

Figure 3. The displacement δR from the K point of the magnetically scattered neutron intensity maxima for $RbFe_{(1-x)}Mg_xCl_3$ (x = 0.02, 0.03 and 0.05) as a function of temperature. Data for pure $RbFeCl_3$ are included for comparison, and were taken from the paper of Wada *et al* (1982).

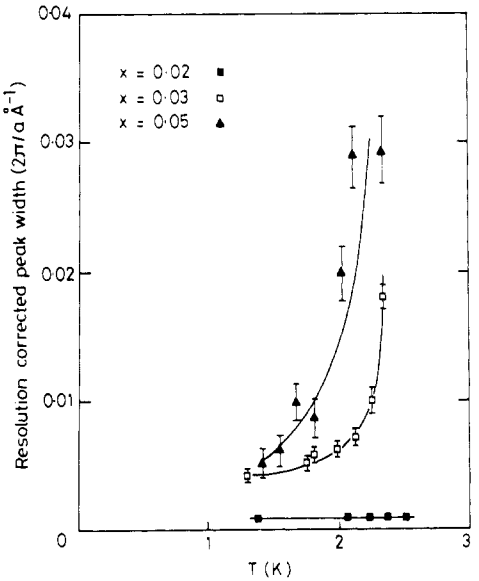

Figure 4. The dependence of the resolution-corrected peak width on temperature and composition for samples of $RbFe_{(1-x)}Mg_xCl_3$ (x = 0.02, 0.03 and 0.05). Note that the data for the x = 0.02 sample depend very much on our estimate of the resolution width, the uncertainty in which is not accounted for in the energy bars on the data points.

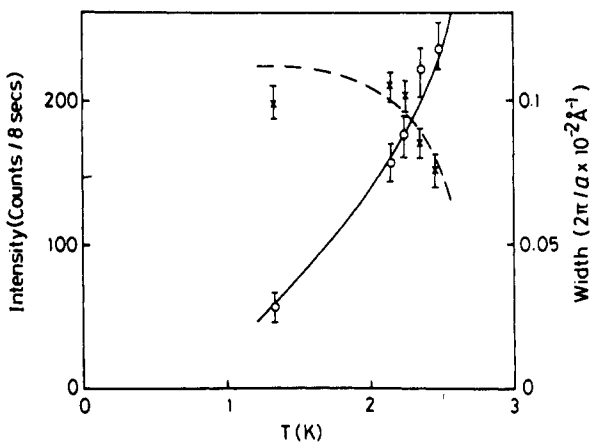

Figure 5. The dependence of the height (×) and width (○) of the diffuse scattering intensity observed near the K point of $RbFe_{(1-x)}Mg_xCl_3$ (x = 0.02). Intensities have been scaled as for figure 2, and all the parameters were derived by least-squares-fitting Lorentzian curves convoluted with the Gaussian resolution function. The curves drawn through the experimental points are merely a guide to the eye, the full curve tracing the width, and the broken curve the intensity.

both the distinct and the diffuse scattering intensity. The heights and widths of the curves describing the diffuse component are presented in figure 5. The diffuse component could not

be fitted to a Gaussian peak and we did not attempt to fit it to more sophisticated lineshapes such as Lorentzian plus Lorentzian-squared functions (Birgeneau *et al* 1984) because of the large number of independent variables already used to describe the scattering profiles. We return to the spatial distribution of this component of the scattered neutron intensity in the next section.

4. Discussion

The change in the magnetic ordering of $RbFeCl_3$ when it is doped with $RbMgCl_3$ is quantitatively very similar to the effect of doping with $CsFeCl_3$ or $RbFeBr_3$: small amounts of dopant destroy the magnetic long-range order found in the pure compound, and the periodicity of the finite magnetic correlations that remain is similar to that of the C, IC_2 and IC_1 phases of $RbFeCl_3$, depending on the temperature and composition. The balance between incommensurate and commensurate magnetic correlations at low temperatures was displaced towards the former, as shown by the lowering of the temperature of the IC_2–C phase transition, whilst the paramagnetic–IC_1 phase transition temperature remained constant (figure 6).

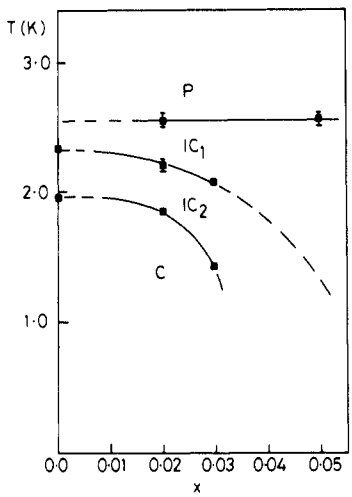

Figure 6. The dependence of the periodicity of the magnetic correlations in $RbFe_{(1-x)}Mg_xCl_3$ ($x = 0.02$, 0.03 and 0.05) as a function of composition and temperature. It must be stressed that the correlations at higher impurity levels are finite in extent, so that these phases differ from those found in the pure chloride—hence the broken curves extrapolated to zero impurity level. Symbols IC_1, IC_2 and C refer to the incommensurate and commensurate periodicities predicted by Shiba (1982). The two lower phase boundaries were not seen down to the base temperature of 1.3 K for the $x = 0.05$ sample, so again the broken curves extrapolate to the phase boundary.

The effect of impurities on the magnetic ordering temperature and the IC–C phase equilibria in $RbFeCl_3$ has been discussed in I and II. It was concluded that existing models cannot adequately describe the reduction of the magnetic ordering temperature of $RbFeCl_3$ in a quantitative manner because they neglect the induced-moment character of the host. In particular, the model of Hone *et al* (1975), which deals with the influence of diamagnetic impurities on the Néel temperature of chains of Heisenberg or Ising moments, weakly coupled by a molecular field, underestimates the fall-off in $T_N(x)/T_N(0)$ with diamagnetic impurity concentration x.

More recently (Harrison 1989), a simple molecular field model has been used to study the effects of diamagnetic dilution on an induced-moment magnet (DIMM). The DIMM model involves setting up a randomly-diluted collection of singlet–doublet sites, with a singlet–doublet splitting D, on one- two- or three-dimensional lattices of various connectivities and joined to other active sites with magnetic exchange constants J. All active sites are given a uniform initial moment then each moment in the lattice is taken in turn and a new value calculated in the exchange field supplied by the neighbouring moments. This process is repeated until the moments attain self-consistent values. Here we use this model to calculate the mean magnetic moment per Fe^{2+} ion in $RbFe_{(1-x)}Mg_xCl_3$ at $T = 0$ as a function of x using values of J_1, J_2 and D derived from inelastic neutron scattering measurements of the dispersion of magnetic excitations in $RbFeCl_3$ (Yoshizawa *et al* 1983). We chose an interpretation of the data that was based on a molecular field excitonic model rather than a more realistic model that took account of short-range magnetic correlations (Suzuki 1983) because the DIMM model also uses the molecular field approximation. It is clear that the fall-off in mean magnetic moment at $T = 0$ with x is very rapid (figure 7). This is probably more informative than deriving the dependence of $T_N(x)/T_N(0)$ because there are several magnetic ordering temperatures for $RbFeCl_3$ and the magnetically 'ordered' phase appears to lack long-range magnetic order in the case of the $x = 0.03$ and 0.05 samples, and perhaps also the 0.02 sample. The extension of this model to finite temperatures requires a proper treatment to be made of the influence of magnetic fluctuations and excitations on the ordering processes. Furthermore, we assume that the diamagnetic impurities are distributed homogeneously throughout the crystal and do not show any chemical clustering. The validity of such an assumption could be checked by Mössbauer spectrometry, as performed on $CsFe_{(1-x)}Mg_xCl_3$ (Lai and Ward 1988).

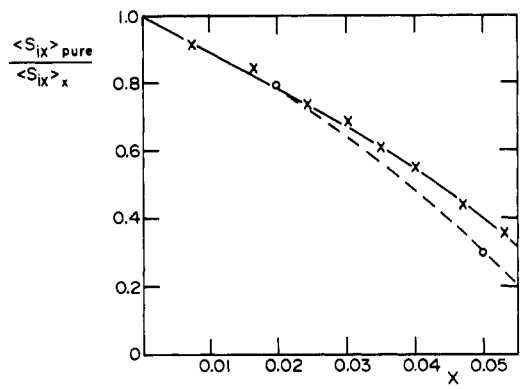

Figure 7. The dependence on composition x of the mean magnetic moment at $T = 0$, expressed as a proportion of the pure moment and calculated using the DIMM model. The exchange parameters and single-ion anisotropy are those derived by Yoshizawa *et al* (1983) for $RbFeCl_3$ and the calculation was performed for a hexagonal lattice of 1000 sites, averaged over several starting configurations. A comparison is made with experimental data derived from figures 2(*a*) and 4 at 1.38 K, depicted as circles. The broken curve through these circles merely provides a guide to the eye.

Despite its simplicity, the DIMM model provides some insight into the behaviour of $RbFe_{(1-x)}Mg_xCl_3$. It demonstrates that on dilution with diamagnetic impurities, not only is the number of active sites reduced, but also the magnitude of the moments on those sites is greatly diminished. It also gives a picture of the spatial distribution of the magnetic moments in the dilute materials. Figure 8 shows the effect of doping a square lattice of singlet–doublet

sites with 1, 2 and 4% of diamagnetic impurities. In the 4% sample we see that statistical fluctuations in the distribution of diamagnetic impurities give rise to relatively large regions where there are no diamagnetic impurities and where the moments are almost as large as in the pure material. These 'islands' of large moments are surrounded by a distribution of much smaller moments. As the temperature is raised from zero the smaller moments melt first, leaving frozen moments on the islands in the form of superparamagnetic clusters. Thus, we expect that as the concentration of the diamagnetic impurity is increased, the intensity of the magnetic scattering of neutrons in the region of the K point at $T = 0$ will rapidly fall, and that some elastic magnetic scattering will remain at temperatures up to the Néel temperature of the pure compound.

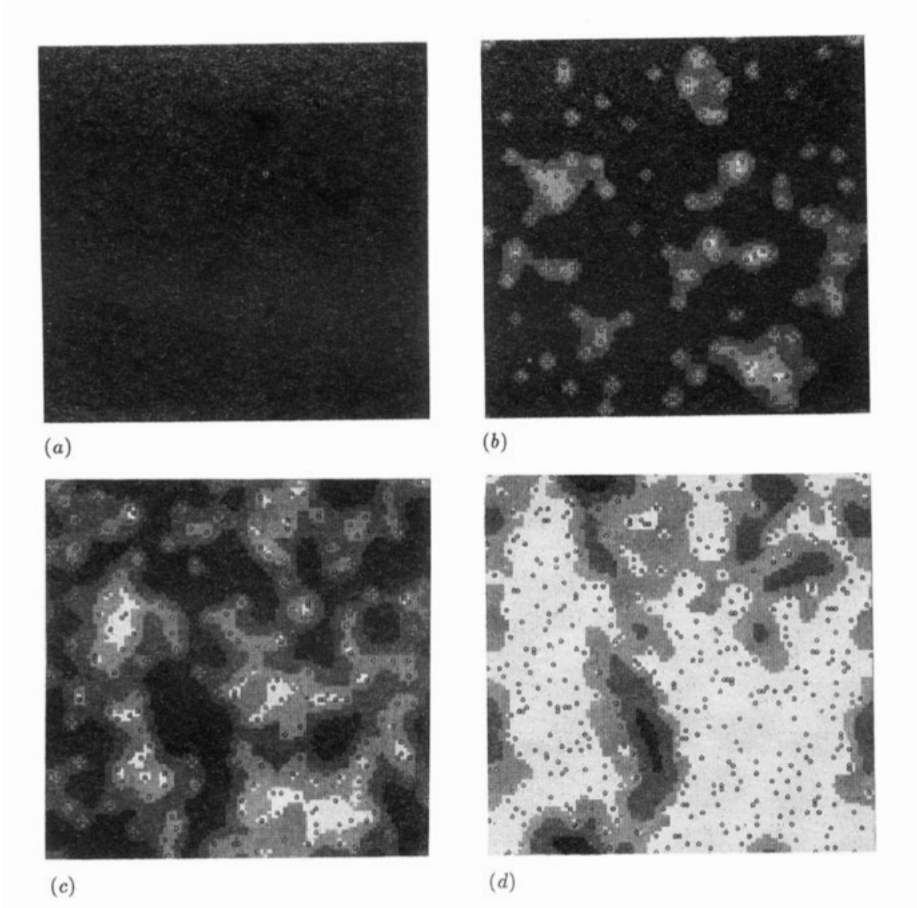

Figure 8. The distribution of induced moments on a square lattice of side 100 containing active sites in which the ratio of single-ion anisotropy to exchange field is just 2% above the critical value below which the pure magnet shows no induced moment. (*a*) depicts the pure lattice and (*b*)–(*d*) lattices with 1, 2 and 4% diamagnetic impurity. The magnitude of the moments at each sites is depicted in quartiles as a fraction of the moment in the pure magnet. For example, the darkest shade corresponds to moments that are (0.75–1.00) times those in the pure material.

Figure 7 illustrates clearly the large reduction in the observed ordered moment at low temperatures as x is increased. Note that the experimental points included in this figure differ from those in figure 2(*a*) in that they have been modified to take account of the increase in the widths of the scattering maxima and therefore they give a more direct measure of the average

ordered moment. The reduction in the size of the regions of large moments is implied in figure 4: for the finite region displayed for the $x = 0.02$ sample, relatively large ordered moments percolate; for the $x = 0.03$ sample such moments are confined to small isolated clusters. Uncertainties remain: the contribution of the smaller moments to the neutron scattering is not given explicitly, nor are we able to be precise about the change in the character of the magnetic phase transitions on doping. Figure 2(*a*) shows that the first-order C–IC_2 phase transition seen in pure $RbFeCl_3$ rapidly broadens on dilution but, until a full Monte Carlo simulation is performed, we have no means of quantifying such effects.

The application of a magnetic field H_z parallel to the crystal c axis is expected to compensate to some extent for the disruptive influence of the dopant. Experimental work (I) and computer simulations (Harrison 1989) have shown that such a field raises the mean of the magnetic moments and reduces the variance. In figure 9(*a*) we display a schematic magnetic H_z–T phase diagram for a pure induced-moment magnet governed by the molecular field approximation. As H_z is increased, the induced moment is increased until the field pulls the moment out of the x–y plane. In 9(*b*) we illustrate the influence of small amounts of diamagnetic impurities, producing the continuous range of moments denoted by the shaded area whose upper boundary is close to that of the pure material. As the concentration of diamagnetic impurities is increased, the shaded region increases in width and both boundaries are lowered until (figure 9(*c*)) almost all of the magnet is like a pure singlet ground state material such as $CsFeCl_3$ (figure 9(*d*)).

Suppose a sample of $RbFe_{(1-x)}Mg_xCl_3$ of composition $x = 0.05$–0.10 was cooled to low temperatures and then a significant magnetic field H_z was applied parallel to the c axis. The 'zero-field-cooled' state that existed before the field was applied is one in which the larger moments are frozen in superparamagnetic clusters. These clusters grow when H_z is applied until they are separated only by narrow domain walls. The merging of domains may require much reorganization and at low temperatures may occur on a timescale that is long enough for it to be observable in a neutron scattering experiment. The growth could be followed by scanning through the elastic scattering intensity in the region of the K point.

A comparison between the different influences of the dopants Cs^+, Mg^{2+} and Br^- on the magnetic ordering processes of $RbFeCl_3$ sheds some light on the influence of each dopant at a microscopic level. In figure 10 we present a plot of the maximum inverse peak width for the magnetically scattered neutron intensity near the K point, as a function of temperature and the concentration of the dopant. This implies that a hierachy of disruptive power of the various dopants may be set up as follows:

$$Br^- > Cs^+ > Mg^{2+}.$$

The relative influences of Br^- and Mg^{2+} are also implied in figure 2(*a*).

The Mg^{2+} ion replaces the Fe^{2+} ion on a one-to-one basis, severing the intrachain superexchange link. However, $RbFeCl_3$ is not particularly one-dimensional ($J_2/J_1 \simeq 10^{-1}$) so the effect of this substitution is much less severe than in most other pseudo-one-dimensional magnets (Takeda and Schouten 1981). Cs^+ ions appear to remove or reduce moments on Fe^{2+} on a much greater than one-to-one basis as quantified either in figure 10 in terms of the diffraction peak widths or in terms of the reduction in scattering intensity at the magnetic Bragg positions with dopant concentration is increased. When a Rb^+ ion is replaced by a larger Cs^+ ion a local structural distortion will probably occur and there will also probably be a local reduction in J_2 and consequently in the ratio J_Q/D. A comparison between the values of J_1, J_2 and D for $RbFeCl_3$ and $CsFeCl_3$ (Visser and Harrison 1988) reveals that D and J_1 do not change very much with composition but J_2 does, being greater for $RbFeCl_3$ by a factor of about 1.8.

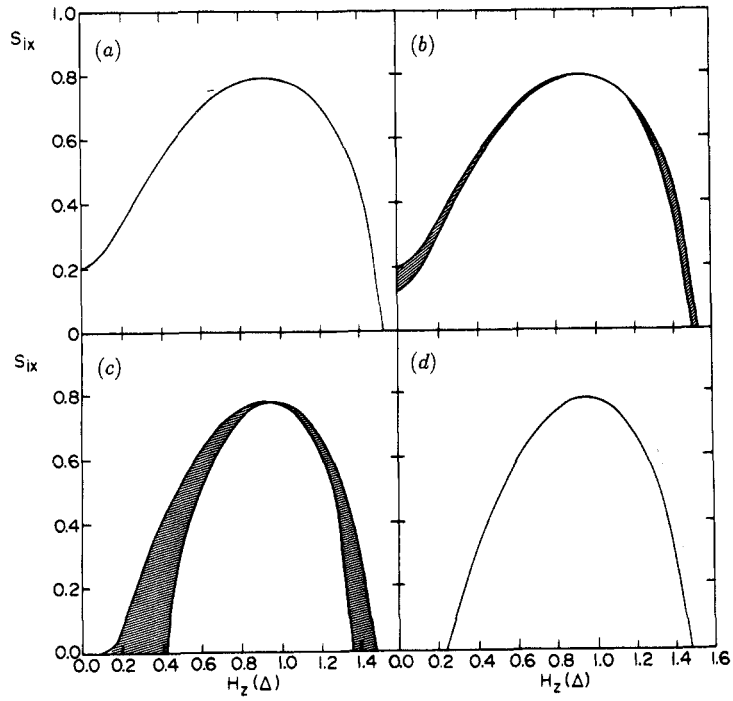

Figure 9. The dependence of the size of the induced moments S_{ix} in a selection of induced-moment magnets similar to $RbFe_{(1-x)}Mg_xCl_3$ as a function of the magnetic field H_z applied parallel to the z direction. (*a*) depicts the change in the homogeneous moment with H_z in a magnet such as $RbFeCl_3$ which possesses a moment in zero applied magnetic field, and (*b*) and (*c*) depict the effect of increasing amounts of diamagnetic dopant on the distribution of moments in such a material, producing a range of values of increasing variance and decreasing mean as the concentration of dopant increases. (*d*) shows the dependence of mean moment on H_z for a magnet such as $CsFeCl_3$ which has zero induced moment when H_z is zero.

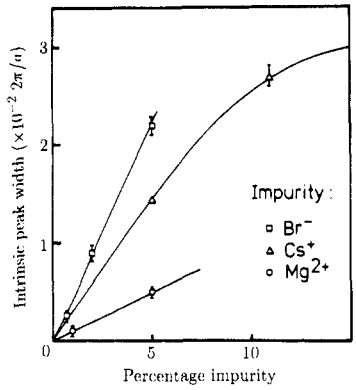

Figure 10. The dependence on the sample composition of the maximum magnetic correlation length (expressed here as its reciprocal value) in all of the doped compounds based on $RbFeCl_3$. These values were measured at 2–2.2 K, depending on the temperature at which the minimum resolution-corrected peak widths lay. The full curves merely provide a guide to the eye, and values at low dopant levels should be treated with caution: their error bars are underestimated, since they include no measure of the uncertainty in the instrumental resolution width.

The replacement of Cl^- ions in the interchain superexchange bridges by Br^- ions will probably increase J_2 slightly. It is also likely that the substitution of Cl^- ions by Br^- ions in the intrachain exchange bridges changes it from a positive value to a smaller positive value or a negative value, reducing J_Q locally and consequently reducing the size of the induced moments on neighbouring ions. A very small proportion of intrachain bridges may have *antiferromagnetic* exchange so may cause greater disruption of the ordered spin structures of $RbFeCl_3$. If we compare figure 4 with the plot of the dependence of the scattering maxima peak widths for $RbFeCl_{(3-x)}Br_3$ in II, we see a marked difference. The widths of the peaks in $RbFeCl_{(3-x)}Br_3$ pass through a minimum as the temperature is reduced, implying a *reduction* in the length of the C or IC_1 magnetic correlations when the samples are cooled below about 1.8 K. The samples of $RbFe_{(1-x)}Mg_xCl_3$ all show a monotonic change in width with temperature down to the lowest experimental value. One interpretation of this result is that the freezing of the smaller moments in $RbFeCl_{(3-x)}Br_3$ at lower temperatures—that is, the moments which are connected to neighbouring moments through bridges with one or more bromine atoms—introduces disorder (Aeppli *et al* 1982). No such source of disorder is expected in $RbFe_{(1-x)}Mg_xCl_3$.

The influence of impurities on the balance between J_2 and γ in $RbFeCl_3$ doped with $RbFeBr_3$ was discussed in II, as was the nature of the diffuse scattering observed near the K point of those materials. The following two reasons for the form of the diffuse scattering in mixed compounds based on $RbFeCl_3$ were postulated there.

(i) Impurities break the spin structure up into smaller domains with the 120° antiferromagnetic spin structure of the pure magnet at low temperatures. The diameter of these domains may be estimated from the neutron diffraction peak widths to be of the order of 50 Å.

(ii) The frustration inherent in the 120° spin structure may be released near impurities, causing local canting of moments and producing a distribution of canting angles centred on the angle of the pure magnet (Villain 1979, Harrison 1987). Canting will also occur near domain walls.

The anisotropic nature of the scattering intensity in the $l = 1$ plane would appear to rule out interpretation (i) as the sole origin of the diffuse scattering. Furthermore, local canting of moments may be the reason why the diffuse scattering component appears to persist to temperatures above T_N. First, let us consider the moments to be classical and not have an induced-moment character. Local canting of moments in the nearest-neighbour shell about a diamagnetic impurity causes them to adopt orientations relative to moments in the next-nearest shells that are closer to the 180° angle that maximizes the pairwise exchange energy. Thus, the exchange field experienced by next-nearest-neighbour moments increases and consequently the temperature at which the correlation between such moments is destroyed is higher. Of course in the induced-moment case the size of the moments in nearest-neighbour shells will also be reduced in size as their exchange field is decreased and the net influence on the exchange field acting on next-nearest neighbours will depend on J_1, J_2 and D and would have to be calculated explicitly.

A similar type of diffuse neutron scattering has recently been seen in other pure and dilute frustrated magnets. The pure hexagonal XY antiferromagnet $CsMnBr_3$, as well as samples doped with the diamagnet $CsMgBr_3$, show a significant elastic, diffuse neutron scattering component centred at $(\frac{1}{3}\ \frac{1}{3}\ 1)_N$ at temperatures between T_N and $3T_N$ (Visser and McIntyre 1987, Visser *et al* 1988). The spatial distribution of this scattering adopts the same form in the $l = 1$ plane as that seen in the $l = 0$ plane of $RbFe_{(1-x)}Mg_xCl_3$. Similar observations have been made in $TlFeCl_3$ (Visser and Knop 1984), a pseudo-one-dimensional ferromagnet whose magnetic properties resemble those of pure $RbFeCl_3$. In all these compounds the single-ion

anisotropy confines the magnetic moment to the a–b plane and the interchain magnetic exchange directs the magnetic scattering of neutrons towards $(\frac{1}{3}\ \frac{1}{3}\ l)_N$. For the pure and doped $CsMnBr_3$ samples it was also found that a small amount of diffuse elastic scattering persisted below T_N. In a magnetization study of $RbFeCl_3$ (Kato *et al* 1985), remanent magnetic behaviour was found in the C phase. One interpretation given to this observation was that it arose from moments trapped between domains in the magnetically frustrated ground state. No indication of this effect was seen in the neutron scattering measurements of Wada *et al* (1982), though Kato *et al* (1985) thought it unlikely that such a type of experiment would detect it.

5. Conclusions

The induced-moment character of $RbFeCl_3$ sensitises it towards doping with diamagnetic impurities, causing the reduction of T_N with impurity concentration to be greater than that predicted by models in which classical moments are coupled by a molecular field. A qualitative explanation of the neutron scattering measurements is given by a simple molecular field calculation that takes account of the induced-moment character of the Fe^{2+} sites. It also provides a picture of the spatial distribution of the moments: at all but the lowest values of x the majority of moments are very small, but islands of moments whose magnitudes are comparable with those in the pure $RbFeCl_3$ remain. This is consistent with the experimental observation that the doped materials contain finite regions of moments with orientations similar to those in the pure material which remain frozen at temperatures comparable with the ordering temperature of the pure material. The model is unable to predict what contribution the smaller moments make to the neutron scattering, nor does it elucidate the the strong elastic diffuse scattering component centred at the K point that persists to temperatures well above T_N. The treatment of such effects would require a full Monte Carlo simulation to be made.

A possible explanation for the diffuse scattering is the canting of moments near impurities, driven by the release of magnetic frustration. This could be studied further by Mössbauer spectrometry, which provides a measure of $\langle \sin^2 \theta \rangle$ (where θ is the angle between nearest-neighbour moments). At temperatures below T_N the induced-moment character of the host material is expected to greatly complicate canting models, as it produces a wide distribution of moment sizes. Such complications could be greatly reduced by repeating the measurements in doped materials subjected to a magnetic field H_z parallel to the crystal c axis, making the variance in the distribution of moment magnitudes much smaller. The application of H_z might also be used to study the relaxation of frozen magnetic disorder (I).

Thus, $RbFe_{(1-x)}Mg_xCl_3$ may not only be used to rationalize the complicated disordering phenomena observed in $Rb_{(1-x)}Cs_xFeCl_3$ and $RbFeCl_{(3-x)}Br_x$, but it might also be used to model a number of problems concerning ordering in inhomogeneous materials. Along with similar materials derived from the induced-moment magnets $RbFeBr_3$ and $TlFeCl_3$ it appears to be the only insulating magnet suitable for a study of bootstrap percolation (Branco *et al* 1988, Harrison 1989).

Acknowledgments

The authors are grateful to the Institut Laue–Langevin for technical support and assistance during the experiments and in particular to G J McIntyre and K R A Ziebeck (now at the Department of Physics at Loughborough University of Technology). They would also like to thank the UK Science and Engineering Research Council for financial support and AH wishes to thank St John's College, Oxford for further financial aid.

References

Aeppli G, Shapiro S M, Birgeneau R J and Chen H S 1982 *Phys. Rev.* B **25** 4882
Birgeneau R J, Cowley R A, Shirane G and Yoshizawa H 1984 *J. Stat. Phys.* **34** 817
Bontemps N, Grisolia C, Nerozzi M and Briat B 1982 *J. Appl. Phys.* **53** 2710
Branco N S, de Queiroz S L A and dos Santos R R 1988 *J. Phys. C: Solid State Phys.* **19** 1909
Eibschutz M, Lines M E and Sherwood R C 1975 *Phys. Rev.* B **11** 4595
Fishman S and Aharony A 1979 *Phys. Rev.* B **19** 3776
Harrison A 1987 *J. Phys. C: Solid State Phys.* **20** 6281
—— 1989 *J. Phys.: Condens. Matter* **1** 6695
Harrison A and Visser D 1989 *J. Phys.: Condens. Matter* **1** 733
Harrison A, Visser D, Day P, Knop W and Steiner M 1986a *J. Phys. C: Solid State Phys.* **19** 6811
Harrison A, Visser D, Day P and Ziebeck K R A 1986b *J. Magn. Magn. Mater.* **54–7** 1273
Hone D, Montano P A, Tonegawa T and Imry Y 1975 *Phys. Rev.* B **12** 5141
Kato H, Tomikawa T, Amaya K and Wada N 1985 *J. Phys. Soc. Japan* **54** 3942
Katsumata K, Nire T, Tanimoto M and Yoshizawa H 1982 *Phys. Rev.* B **25** 428
Knop W, Steiner M and Day P 1983 *J. Magn. Magn. Mater.* **31–4** 1033
Lai K K and Ward J B 1988 *J. Phys. C: Solid State Phys.* **21** 2279
Lines M E and Eibschutz M 1975 *Phys. Rev.* B **11** 4583
Munninghof G, Hellner E, Treutmann W, Lehner N and Heger G 1984 *J. Phys. C: Solid State Phys.* **17** 1281
Seifert H-J and Fink H 1975 *Rev. Chim. Miner.* **12** 466
Shiba H 1982 *Solid State Commun.* **41** 511
Shiba H and Suzuki N 1983 *J. Phys. Soc. Japan* **52** 1383
Suzuki N 1983 *J. Phys. Soc. Japan* **52** 3907
Takeda K and Schouten J C 1981 *J. Phys. Soc. Japan* **50** 2554
Villain J 1979 *Z. Phys.* B **33** 31
Visser D and Harrison A 1988 *J. Physique* C **8** 1467
Visser D, Harrison A and McIntyre G J 1988 *J. Physique Coll.* C **8** 1255
Visser D and Knop W 1984 unpublished results
Visser D and McIntyre G J 1987 *Annual Report of the Institut Laue–Langevin*
Wada M, Ubukoshi K and Hirakawa K 1982 *J. Phys. Soc. Japan* **51** 283
Yoshizawa H, Kozukue W and Hirakawa K 1983 *J. Phys. Soc. Japan* **52** 1814
Zodkevitz A, Makovsky J and Kalman Z H 1970 *Israel. J. Chem.* **8** 755